Numerical Investigation of Vortex Breakdown Control by Along-the-Core Blowing in Transonic Flows

Michael Werner*† and Nico Hartmann*

*German Aerospace Center (DLR), Institute of Aerodynamics and Flow Technology
Department of High Speed Configurations, 37073 Göttingen, Germany
michael.werner@dlr.de

†Corresponding author

Abstract

The current study numerically investigates the use of active flow control to influence the stability of leading edge vortices on a generic multi-swept delta wing at transonic conditions. The method chosen for the current investigation is the so-called along-the-core blowing, where a jet is used to inject additional axial momentum into the vortex core of one of the leading edge vortices by constant blowing. Two different Mach numbers, Ma = 0.55 and Ma = 0.85 are taken into consideration. The angle of attack is varied between $\alpha = 12^{\circ}$ and $\alpha = 24^{\circ}$. At Ma = 0.55 the simulations show a noticeable delay or even complete suppression of vortex-breakdown of the actuated vortex across the whole range of investigated angles of attack, whereas the effect of the actuation is less pronounced at Ma = 0.85. Overall, the delay of vortex breakdown leads to an increase in lift coefficient of between 5% and 10% at Ma = 0.55, and between 2% and 5% at Ma = 0.85.

1. Introduction

One of the core requirements of modern combat aircraft is high maneuverability at high speeds. Therefore, most of these aircraft rely on highly swept wings, so-called delta wings. A special feature of this type of wing is the development of strong vortices along the leading edge at moderate to high angles of attack. An enhancement of the classical delta wing are the so-called multi-swept delta wings that feature a segmented leading edge with multiple different leading edge sweep angles. This leads to the development of multiple vortices, that might interact with each other. Additionally, at transonic Mach numbers shocks develop above the wing, that might interact with, and thereby destabilize, the leading edge vortices^[15]. Generally, the strength of the leading edge vortices increases with increasing angle of attack (AoA), until a critical point is reached and vortex-breakdown occurs^[10]. Vortex-breakdown is typically signified by an increase in vortex radius, the reduction of its circumferential velocity component and the development of an area of recirculating flow in the vortex core. Once vortex breakdown occurs, the vortices lose their coherence, which leads to the loss of their associated lift. This in turn might induce strong forces and moments that in turn influence the stability and control characteristics of the aircraft. This is why there is a strong interest in the development of techniques to stabilize the vortices and delay or even eliminate vortex breakdown using flow control devices.

The current generation of combat aircraft typically uses control surfaces, such as canards or leading edge slats and flaps to influence the characteristics of the leading edge vortices^[7]. These methods are established and generally well understood. However, control surfaces contain movable parts under high mechanical loads, and the deflection of the control surfaces can negatively influence the detectability of the aircraft. This is why there is also a growing interest in using fluidic active flow control (AFC) techniques, such as blowing and suction, to influence the flow^[12].

A broad overview of the different available approaches is given by Gursul et al. [4] and Gursul and Wang [3]. With respect to the application of AFC to vortex-dominated flows, there are generally two possible goals: on the one hand, AFC can be used to increase the strength of the vortices, leading to lift enhancements at low angles of attack, but also to premature vortex breakdown at moderate angles of attack. This is typically achieved by using techniques such as leading edge blowing or suction. On the other hand, AFC can be used to stabilize the vortices, which delays vortex breakdown and thereby shifts the flight envelope to higher angles of attack. In their review, Gursul et al. [4] compared the efficiency of different techniques with respect to the delay of vortex breakdown for a given blowing coefficient c_{μ} . They found that the most energy efficient technique for the delay of vortex breakdown is the so-called along-the-coreblowing (ACB). The basic idea of this technique is to accelerate the flow in the vortex core by injecting a jet directly

into the core of the leading edge vortex. This increases the axial momentum of the vortex, which has a stabilizing effect as it helps to overcome the negative pressure gradient associated with the occurrence of vortex breakdown^{[13],[14]}. However, in literature, most applications of ACB were limited to lowspeed flows, where it is easier to increase the axial momentum of the vortex due to the overall lower flow speeds. One example of the application of ACB to transonic flows is given by Kurade et al.^[8]. They studied the effect of spanwise blowing and along-the-core blowing on vortex breakdown experimentally at Mach numbers between Ma = 0.7 to Ma = 1.2. In their study, they observed an increase in lift of 6% - 9%, with the best results being achieved by using a sonic jet.

For the current study, the application of ACB to delay vortex breakdown is investigated numerically on a multiple-swept delta wing at transonic speeds. The goal of the current study is to identify a suitable actuation concept for use in a subsequent experimental investigation, and to assess the effectiveness of AFC in delaying vortex breakdown at transonic speeds. The geometry chosen for the current investigation is the so-called DLR-F23 configuration that was designed during the DLR research project Diabolo^[9]. The flow field around the DLR-F23 configuration has been previously studied both experimentally and numerically by Zastrow et al.^[19] and Hartl et al.^[5]. In addition to the current study, the DLR-F23 configuration is also currently used to investigate the effect of tail-buffeting within the DLR research project Wingmates^[6].

2. Description of Test Case

In this section, an overview over the setup of the current test case is given. The investigated geometry and the flow conditions are introduced in section 2.1, whereas the numerical setup and mesh generation is described in section 2.2. Finally, the modeling of the actuation jet is introduced in section 2.3.

2.1 Geometry and Flow Conditions

The geometry under investigation is the so-called DLR-F23 configuration, shown in Figure 1. The DLR-F23 is a generic multi-swept delta wing with leading edge sweep angles of $\varphi_1 = 45^\circ$, $\varphi_2 = 75^\circ$ and $\varphi_3 = 45^\circ$ for the levcon, strake and main wing, respectively, and a highly swept ogival forebody. The wing itself features a symmetric elliptical profile, and the leading and trailing edges of the configuration feature a radius of r = 0.5 mm. The geometry has a half span of s = 0.42 m, a root chord of $c_r = 0.575$ m and a total length of 0.862 m. The moment reference point (MRP) is located 0.575 m downstream of the origin at y = z = 0 m, the reference length is $l_{\mu} = 0.382$ m and the reference area is $A_{ref} = 0.133$ m². For the analysis of the surface pressures on the wing, six different cut positions at different chordwise positions are defined, as indicated in Figure 1. However, in the current paper only the cuts S_2 , S_4 and S_6 will be used for analysis.

The flow conditions of the current study are based on the flow conditions of the experimental wind tunnel measurements previously performed in the Transonic Wind Tunnel Göttingen (DNW-TWG) by Zastrow et al. [19]. For all test cases, a total temperature of $T_t = 310 \,\mathrm{K}$ and a total pressure of $p_t = 60 \,\mathrm{kPa}$ are used. Two different Mach numbers are investigated, Ma = 0.55 and Ma = 0.85, with Reynolds numbers based on the reference length l_{μ} of $Re_{l_{\mu}} = 2.32 \times 10^6$ and $Re_{l_{\mu}} = 3.02 \times 10^6$, respectively. As the goal of the current investigation is to delay the onset of vortex breakdown, which starts to occur above the DLR-F23 configuration between $\alpha = 15^\circ$ and $\alpha = 18^\circ$, depending on the Mach number, the angle of attack was varied between $12^\circ \le \alpha \le 24^\circ$.

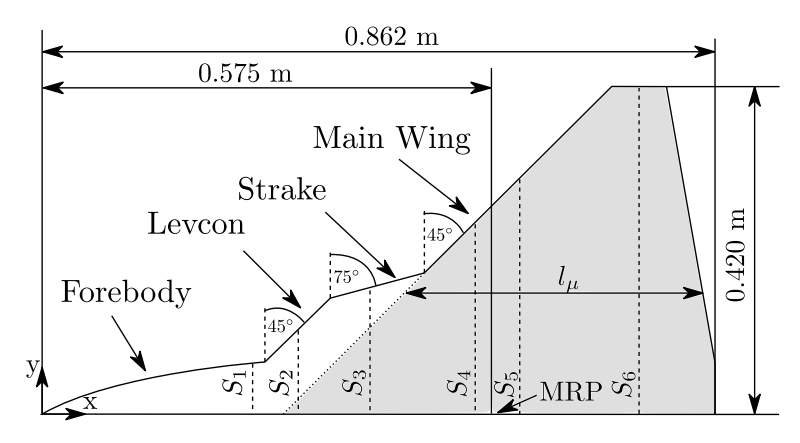
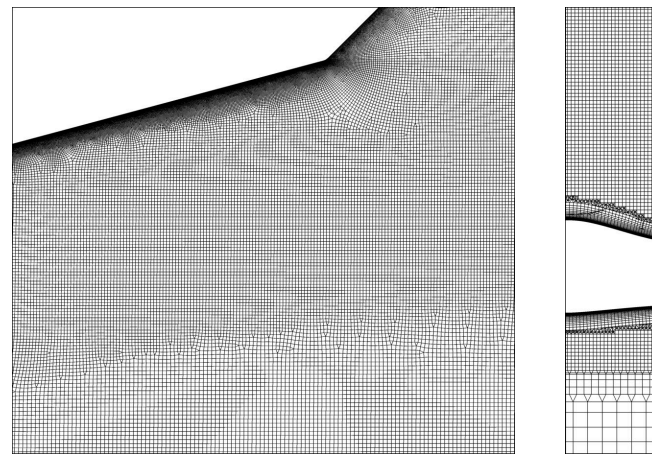


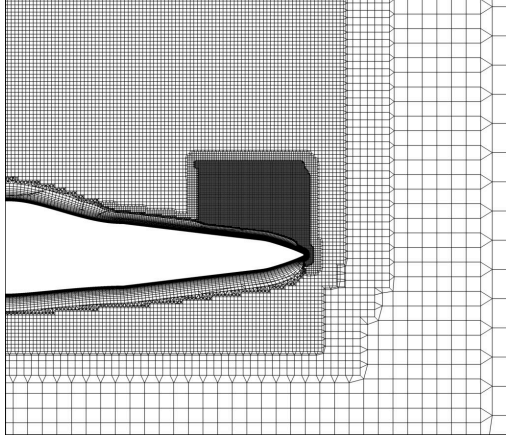
Figure 1: Sketch of the DLR-F23 configuration

2.2 Numerical Setup

The numerical simulations of this study are carried out using the DLR TAU code^[2], a finite-volume solver for computational fluid dynamics (CFD) of three-dimensional, compressible flows on hybrid computational meshes. For the spatial discretization of the Reynolds-averaged Navier-Stokes (RANS) equations, a second-order AUSMDV upwind scheme is used, both for the main flow variables and the turbulence terms. The temporal discretization is achieved using an implicit Backward-Euler approach. Due to the inherent unsteadiness of the investigated flow fields, all results shown in this paper are based on unsteady RANS (URANS) simulations. The time-accurate simulations are performed using a second-order dual-time stepping approach, together with a lower-upper symmetric Gauss-Seidel method for the solution of the inner subiterations. As the highest flow velocities occur in the region of the actuation jet, a time step of 1×10^{-5} s is chosen for all simulations, independent of the farfield Mach number. The convergence of the inner iterations is assessed using a Cauchy convergence criterion based on the coefficients of lift, drag and pitching moment, and the maximum of the Mach number in the field. Convergence is assumed if the residual of the last 20 iterations is below 1×10^{-6} for the lift and drag coefficients, and below 1×10^{-5} for the pitching moment coefficient and maximum Mach number. Based on the findings of previous simulations of the flow field around a very similar configuration^{[18],[17]}, the two-equation Menter SST turbulence model^[11] is chosen to model the turbulence terms.

The computational meshes of the current study are created using the commercial meshing software ANSA^[1]. ANSA is a highly automated mesh generator, that automatically detects relevant geometric features, such as leading and trailing edges, and automatically adjusts the mesh accordingly. The resulting meshes are hybrid meshes with large regions of quasi-structured cells, as can be seen in Figure 2. To better resolve the near-wall boundary layer, a quasi-structured prism grid with 40 layers and a growth rate of 1.2 is used on all solid walls. The first cell height is set to 1.5×10^{-6} m, so that $y^+ \le 1$ is achieved on the whole wing. In order to correctly capture the flow field around the wing, a maximum cell size of 2 mm is prescribed in the region around the wing where vortices and shocks are expected to occur. Additionally, in order to correctly resolve the effect of the actuation jet, the region around the actuation position and the vortex core of the actuated vortex, is further refined with a maximum volume cell size of 0.75 mm. A mesh convergence study, where the cell sizes of the surface and volume mesh were both halfed and doubled, as compared to the original mesh, showed no relevant differences between the medium and fine mesh, which is why the medium mesh, with the previously described mesh settings, is chosen for the remainder of the simulations in this study. The final mesh features about 54×10^6 cells and 43×10^6 points for a half-model configuration.





(a) Surface mesh on the strake

(b) Volume mesh around the strake

Figure 2: Visualisation of the computational grid around the DLR-F23 configuration

2.3 Numerical Modeling of the Actuation Jet

Within this study, the actuation jet is introduced into the computational domain by using a special boundary condition available in the TAU code, the so-called actuation boundary condition, rather than actually modeling the internal piping and the jet nozzle directly. This allows for a quick and easy modification of the jet position, direction and outlet area, without the need to modify the geometry and recreate the computational mesh for each investigated test case. Instead, it is possible to simply assign the boundary condition to a certain subset of the surface cells on the lee side of the wing.

With this approach, the actuation jet is defined by a number of characteristic parameters: the total pressure $p_{0,j}$ and total temperature $T_{0,j}$ of the jet, as well as its Mach number Ma_j and direction, which together are used to calculate the components of the jet velocity \vec{v}_j . Additionally, the area of the surface that defines the actuation boundary condition is an important factor influencing the achievable mass flow rate of the jet. In order to limit the number of free parameters, the jet Mach number and the jet total temperature are fixed for all simulations at $Ma_j = 1.8$ and $T_{0,j} = 300 \,\mathrm{K}$, respectively. Additionally, for the simulations presented in this paper, the area of the actuation boundary was fixed to $A_j = 100 \,\mathrm{mm}^2$ for Ma = 0.55, respectively to $A_j = 50 \,\mathrm{mm}^2$ for Ma = 0.85. This leaves the jet pressure and direction as the two remaining characteristic parameters that are varied throughout this study.

With respect to the seemingly large surface area of the actuation boundary, it is important to note that this is only the surface area on the wing, which corresponds to the projection of an actuation channel, that is inclined by the jet angle θ , on the wing surface. The effective area for the calculation of the mass flow rate is instead defined as $A_{j,eff} = sin(\theta)A_j$, and depends therefore on the direction of the actuation jet. In the remainder of this paper, this effective area is used to calculate the blowing coefficient $C_{\mu} = 2(q_j A_{j,eff})/(q_{\infty} A_{ref})$, where q_j and q_{∞} are the dynamic pressures of the jet and freestream, respectively.

3. Results

In this section, the results of the numerical simulations are presented. First, in section 3.1, the general flow topology around the DLR-F23 configuration at transonic conditions is presented. Next, in section 3.2, the reference simulations without actuation are introduced. Additionally, in this section the choice of the actuation position is discussed. Finally, in section 3.3, the results of the simulations with actuation are presented.

3.1 Basic Flow Topology

A visualization of the basic flow topology around the DLR-F23 configuration at Ma = 0.85, $\alpha = 15^{\circ}$ is shown in Figure 3. There, the wing surface is colored by the pressure coefficient c_P , while the vortical flow is visualized using differently colored streamlines. Generally, three different primary vortices form along the leading edges of the wing: the inboard vortex (shown in red), the midboard vortex (shown in green and orange) and the outboard vortex (shown in black). Further downstream, vortex-vortex interaction, including vortex-merging occurs between the midboard and outboard vortices. Also, at higher angles of attack, vortex-merging of the inboard and midboard vortices can be observed. In addition, at transonic speeds, shocks form above the wing, indicated by yellow dashed lines, leading to the occurrence of vortex-shock interaction.

A special feature of the flow around the DLR-F23 configuration is the fact that the midboard vortex is actually a combined vortex, that is formed by the combination of the separated shear layers originating from the levcon (shown in green) and those of the strake (shown in orange). Specifically, the separated shear layer of the levcon forms the vortex core of the midboard vortex, whereas the shear layer of the strake forms the outer layer. Additional details on the flow topology around the DLR-F23 configuration without actuation are given by Zastrow et al.^[19]

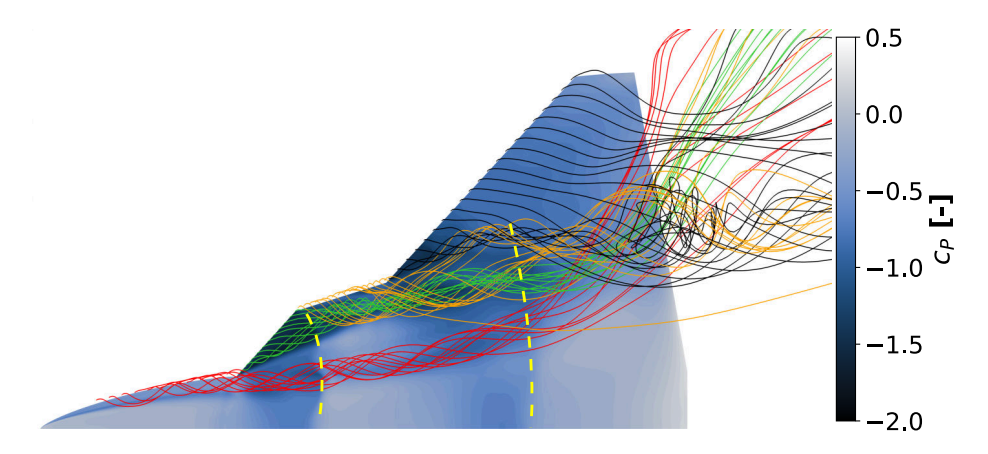


Figure 3: Flow topology above the DLR-F23 configuration visualized using streamlines and pressure coefficient, shock positions indicated using dashed yellow lines, Ma = 0.85, $\alpha = 15^{\circ}$

3.2 Reference Simulations without Actuation

As a first step of the current study, a number of reference simulations without actuation are carried out to assess the flow around the DLR-F23 configuration, to identify suitable actuation positions and to validate the numerical simulations against existing experimental results. The DLR-F23 configuration has been previously experimentally investigated in the scope of the DLR project Diabolo^{[19],[5]}, and the resulting surface pressure data from iPSP measurements was provided by the Department of Aeroelastic Experiments for validation of the numerical results of this study.

A comparison between the experimental surface pressure distribution and the results of the numerical simulations at Ma = 0.55 and Ma = 0.85 is given in Figure 4. The comparison is performed at three different chordwise positions, S_2 , S_4 and S_6 . The exact location of the different chordwise cuts on the model is shown in Figure 1. While there are some differences, for example in the inboard region and with respect to exact strength of the suction peaks of the various vortices, the overall agreement between CFD and experiment is judged as acceptable. Especially the position of the vortices, which is of great importance for the correct orientation of the actuation jet, is predicted very well by the numerical simulations.

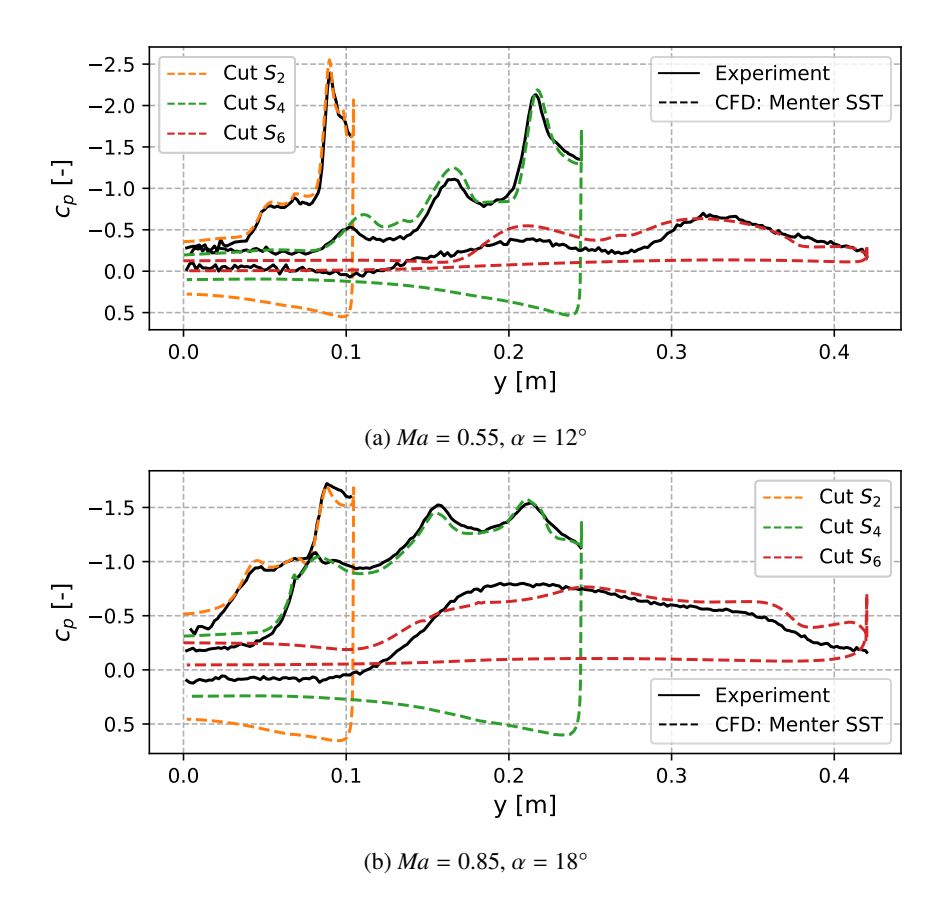


Figure 4: Comparison of the surface pressure coefficient between CFD and experiment for two different Mach numbers at different x-positions above the wing

As described earlier, the basic idea of the along-the-core-blowing requires the actuation jet to be positioned in such a way that it enters the vortex core and thereby increases the axial momentum of the vortex, which has a stabilizing effect on the vortex. For the actual implementation of the actuation it is therefore necessary to identify a position where there is only a limited variation of the vortex core position over a broad range of flow conditions, so that the jet position does not need to be adjusted too much. While this is of lesser importance for the current numerical study, it is a necessary prerequisite for the subsequently planned wind tunnel campaign, where it is not feasible to change the nozzle position for each test case.

In order to identify a suitable position for the actuation jet, the trajectory of the midboard vortex is extracted from the numerical simulations. The identification and tracking of the vortex core is achieved semi-automatically with a predictor-corrector approach^[17], where the starting point on the vortex axis is manually given at a point near the leading edge of the wing, and the subsequent locations of the vortex axis are then automatically determined based on the maximum of the so-called swirl criterion^[16], $Swirl = \vec{\omega} \cdot \vec{v}/\varrho ||\vec{v}||^2$, at different x-positions along the vortex trajectory.

A visualization of the y-position of the vortex core of the midboard vortex for different angles of attack at Ma = 0.55 and Ma = 0.85 is shown in Figure 5. It can be seen that there is only a limited amount of variation of the vortex trajectory above the levcon and strake, $x \le 0.45$ m, as the vortex position in this region is still largely dictated by the leading edge geometry. Only further downstream, above the main wing, larger deviations of the vortex position occur, especially for Ma = 0.85. Based on these results, the center of the actuation jet is chosen to be located at x = 0.405 m, y = 0.14 m for the test cases at Ma = 0.85. respectively at x = 0.412 m, y = 0.137 m for the test cases at Ma = 0.85.

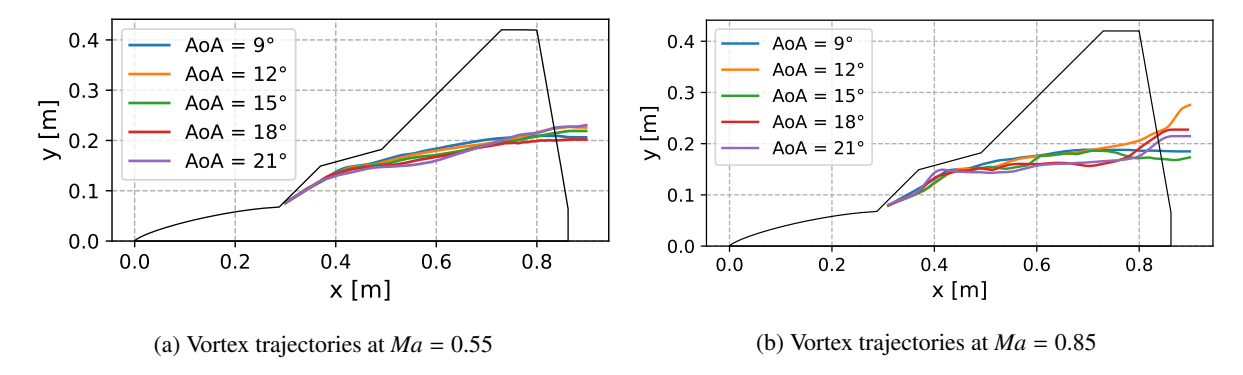


Figure 5: Depiction of the trajectories of the midboard vortex at Ma = 0.55 and Ma = 0.85 for different angles of attack

By positioning the actuation jet at this location, it is possible to utilize a specific feature of the flow around the DLR-F23 configuration. As shown in Figure 3, the midboard vortex consists of the combination of the separated shear layers originating from the levcon and strake, with the levcon shear layer forming the vortex core of the combined vortex. The chosen jet location is positioned far enough upstream that the two shear layers have not yet fully merged, compare Figure 6, where the vortex-merging of the levcon and strake vortices is visualized at two chordwise positions using the normalized Q-criterion, $Q^* = Q(l_\mu^2/U_\infty^2)$. By introducing the actuation jet before the two vortices have merged, one of two possible ways to influence the vortex core can be achieved: if the jet is of moderate strength, the fluid of the jet is caught in-between the two vortices and thereby injected into the vortex core of the midboard vortex without needing to penetrate through the established shear layer of a strong vortex. Otherwise, if the jet is very strong, the actuation can prevent the two vortices from merging, leading to the development of a fresh strake vortex, that doesn't include the levcon vortex as its vortex core. As will be shown in the following section, both ways lead to a stabilization of the midboard vortex and a delay of vortex breakdown.

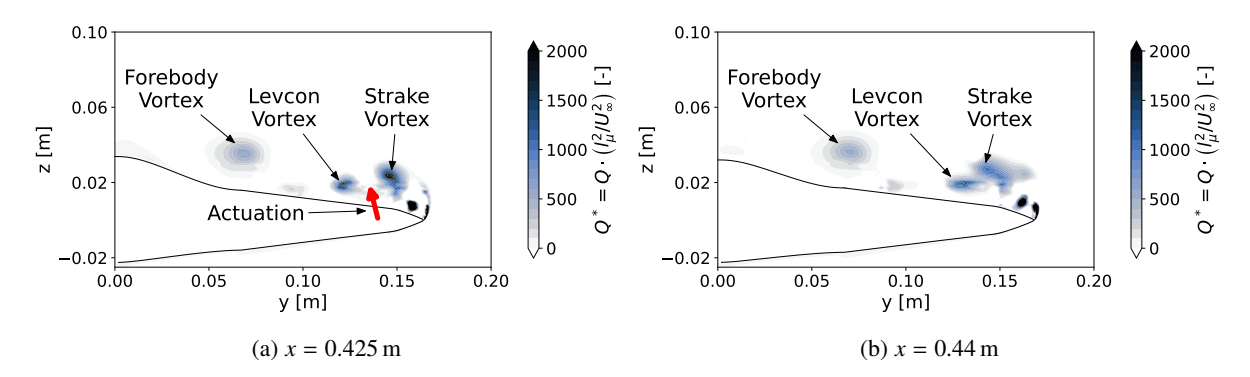


Figure 6: Visualisation of the vortex topology on the strake in two different x-normal planes using the Q-criterion, Ma = 0.85, $\alpha = 15^{\circ}$

3.3 Simulations with Actuation

As the next step of the investigation, a parametric study of the jet parameters is performed based on the findings of the reference simulations. The main parameters that are varied are the total pressure of the jet fluid and the orientation of the jet, given by two angles: θ_v , the angle between the jet axis and the xy-plane, and θ_h , the angle between the jet axis and the xz-plane. Originally, a variation of the Mach number was also planned. However, based on the findings

of some preliminary simulations, and due to the occurrence of numerical issues at lower Mach numbers, the jet Mach number was fixed for the parametric study at $Ma_j = 1.8$. Within the parametric study, θ_h and θ_v are varied between 0° and 20° , and between 30° and 45° , respectively. The total pressure of the jet is originally chosen such that the static pressure at the jet outlet, p_j , matches the static pressure on the wing of the reference simulations, $p_{s,ref}$. Within the parametric study, the jet pressure is then increased to up to four times the static pressure of the reference case, as a means to increase the mass flow rate, and thereby the impulse, of the jet.

As mentioned in the previous section, during this study two different ways to delay vortex breakdown were found. At Ma = 0.55, attempts to directly inject the actuation jet into the vortex core of the midboard vortex were generally not successful. For cases where the jet successfully entered the vortex core, the achieved increase in axial impulse was negligible, as the mass flow rate was typically too low. However, while trying to increase the mass flow rate by increasing the jet pressure p_j , it was found that the actuation prevented merging of the levcon and strake vortices, leading to the development of a separate strake vortex that was more robust to vortex breakdown than the combined midboard vortex of the baseline simulations. Two parameter combinations proved effective in delaying or suppressing vortex breakdown of the midboard vortex: in the first case, the actuation jet is oriented directly along the previously determined vortex axis, $\theta_v = 30^\circ$, $\theta_h = 15^\circ$. In the second case, the actuation jet is oriented slightly against the sense of rotation of the vortex, $\theta_v = 45^\circ$, $\theta_h = 0^\circ$. In both cases, the static pressure of the jet is set to twice the static pressure of the reference simulations, $p_j = 2p_{s,ref}$.

A comparison of the flow topology above the DLR-F23 configuration for cases with and without actuation at Ma=0.55, $\alpha=21^\circ$ is shown in Figure 7. Here, the vortical structures are visualized using a blue isosurface of the normalized Q-criterion, $Q^*=Q(l_\mu^2/U_\infty)=50$. Additionally, the areas of recirculating flow, which indicate the occurrence of vortex breakdown, are shown using a red isosurface of the x-component of the velocity, $v_x=-0.01\,\mathrm{m\,s^{-1}}$. For the reference simulation without actuation, shown in Figure 7a, vortex breakdown of the midboard vortex occurs at approximately half-chord position above the main wing, and the outboard vortex breaks down close to the trailing edge. In Figure 7b the result of a simulation with $p_j=p_{s,ref}$ is shown. For this case, no stabilizing effect on the midboard vortex is observed. Instead, the size of the recirculation bubble is even slightly increased as compared to the reference simulation. In contrast, Figures 7c and 7d show simulations with increased jet pressure, and different orientations of the actuation jet. In both cases, the area of recirculating flow within the midboard vortex, and thereby vortex breakdown of the same, is completely suppressed. In addition, for the case $\theta_v=45^\circ$, $\theta_h=0^\circ$, even the vortex breakdown of the outboard vortex is positively affected due to the stabilizing influence of the midboard vortex.

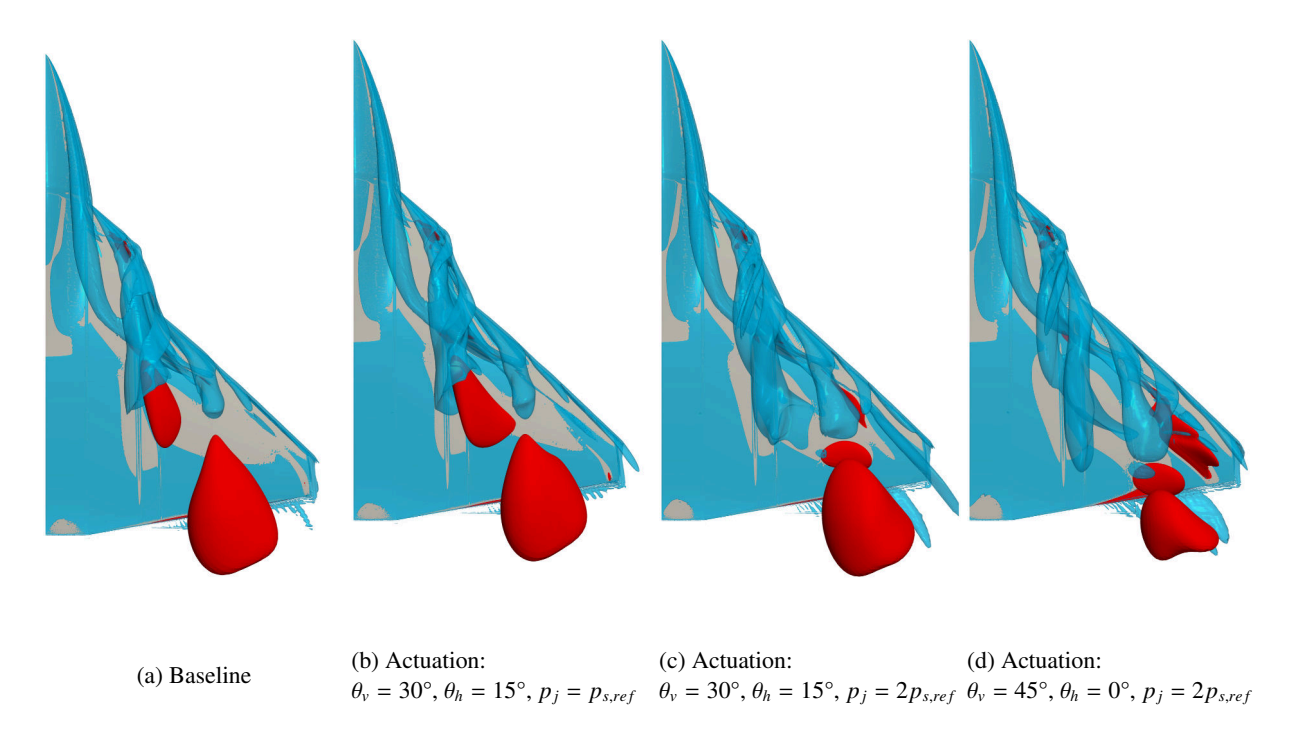


Figure 7: Visualisation of the vortex topology above the wing using an isosurface of the Q-criterion (blue) for cases with and without actuation, areas of reversed flow indicated by isosurface of $v_x = -0.1 \,\mathrm{m \, s^{-1}}$ (red), Ma = 0.55, $\alpha = 21^{\circ}$

To better analyze the effect of the actuation on the flow field within the midboard vortex, Figure 8 shows the development of two quantities, the axial velocity deficit δ and the x-component of the vorticity ω_x , in the vortex core

along the vortex trajectory for cases with and without actuation. In Figure 8a, the development of the velocity deficit is presented. The velocity deficit $\delta = 1 - (v_{x,A}/U_{\infty})$, where $v_{x,A}$ is the x-component of the velocity on the vortex axis, is used to distinguish between jet-type vortices, $\delta < 0$, and wake-type vortices, $0 < \delta < 1$. If $\delta > 1$, this indicates that the velocity in the vortex core is negative, which means that vortex breakdown occurred. For the reference simulation (shown in blue), vortex breakdown occurs at $x \approx 0.59$ m. As was already seen in Figure 7b, for the case $\theta_v = 30^\circ$, $\theta_h = 15^\circ$, $p_j = p_{s,ref}$ (shown in orange) vortex breakdown is only marginally delayed and occurs at $x \approx 0.61$ m. In contrast, the two simulations with increased jet pressure show a noticeable increase in δ downstream of the actuation position at $x \geq 0.425$ m, indicating the disturbance introduced by the strong blowing. However, further downstream the flow in the vortex core re-accelerates, once the new strake vortex is formed, completely preventing vortex breakdown above the wing. In a direct comparison, the actuation with $\theta_v = 45^\circ$ seems to be slightly more effective in reducing the velocity deficit in the vortex core.

Next, in Figure 8b the development of the vorticity ω_x in the vortex core is shown. The vorticity serves as a measure for the strength of the vortex, specifically its circumferential component. Once vortex breakdown occurs, the vorticity decreases to almost zero, as the vortex loses coherence. It can be seen that the development of ω_x is almost identical between the reference case (shown in blue) and the case $\theta_v = 30^\circ$, $\theta_h = 15^\circ$, $p_j = p_{s,ref}$ (shown in orange), again showing that the actuation in this case has almost no effect. The other two cases qualitatively exhibit a very similar behaviour to each other. However, the case $\theta_v = 30^\circ$, $\theta_h = 15^\circ$, $p_j = 2p_{s,ref}$ (shown in green) features slightly lower values of ω_x than the case $\theta_v = 45^\circ$, $\theta_h = 0^\circ$, $p_j = 2p_{s,ref}$ (shown in red), indicating a slightly weaker vortex.

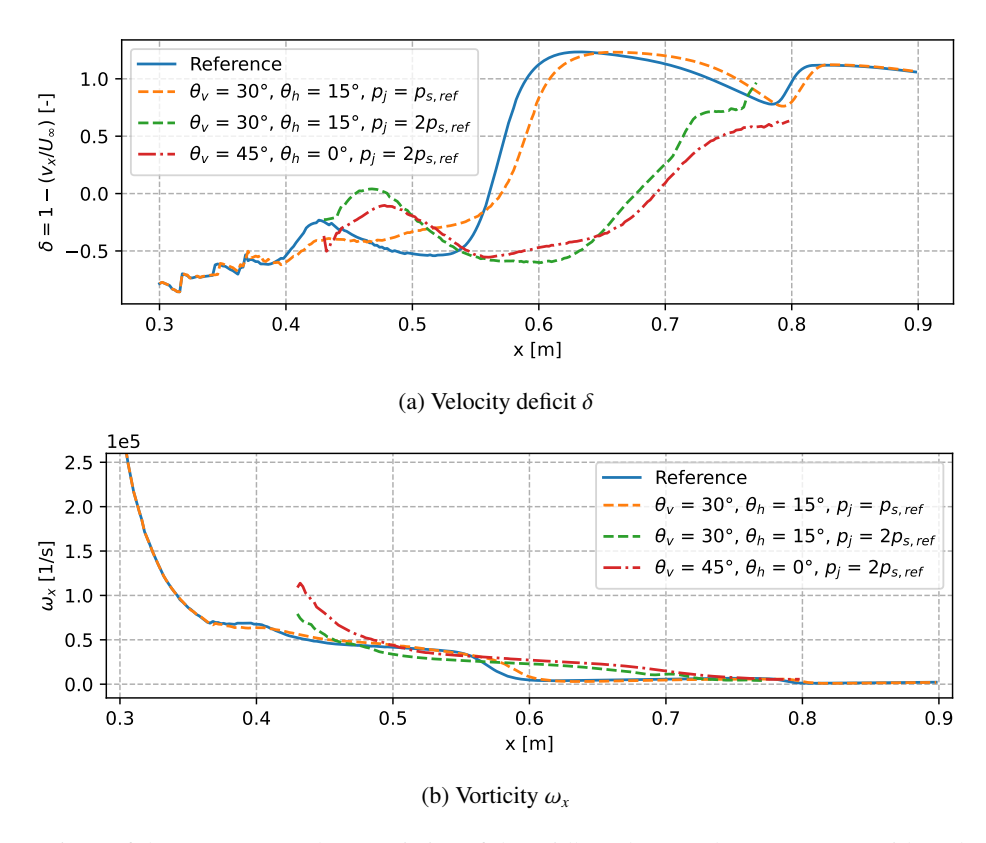


Figure 8: Comparison of the vortex core characteristics of the midboard vortex between cases with and without actuation, Ma = 0.55, $\alpha = 21^{\circ}$

The successful delay of vortex breakdown above the wing positively influences the aerodynamic coefficients of the configuration. This is shown in Figure 9, where lift and pitching moment coefficients are compared between the simulations with and without actuation. It can be seen that, at Ma = 0.55, the actuation leads to a noticeable increase in lift, between 5% and 10%, across the full range of investigated angles of attack, at least for the case with $\theta_v = 45^\circ$. The gain is lower at low angles of attack, as vortex breakdown occurs further downstream at these conditions, and therefore the effect of suppressing vortex breakdown is lower. Additionally, the pitching moment is also positively influenced by the delay of vortex breakdown, as the lift distribution is shifted downstream, leading to lower pitching moment. Only at $\alpha = 24^\circ$ the actuation leads to an increase in pitching moment, as the whole extent of the stabilization of the midboard vortex is located upstream of the MRP. While the two different actuation settings achieve similar maximum improvements to lift at lower angles of attack, it is noticeable that the effect of the setting where the jet is oriented

slightly against sense of rotation of the vortex, $\theta_v = 45^\circ$, $\theta_h = 0^\circ$, $p_j = 2p_{s,ref}$, is more consistent across varying angles of attack, and also effective at higher angles of attack.

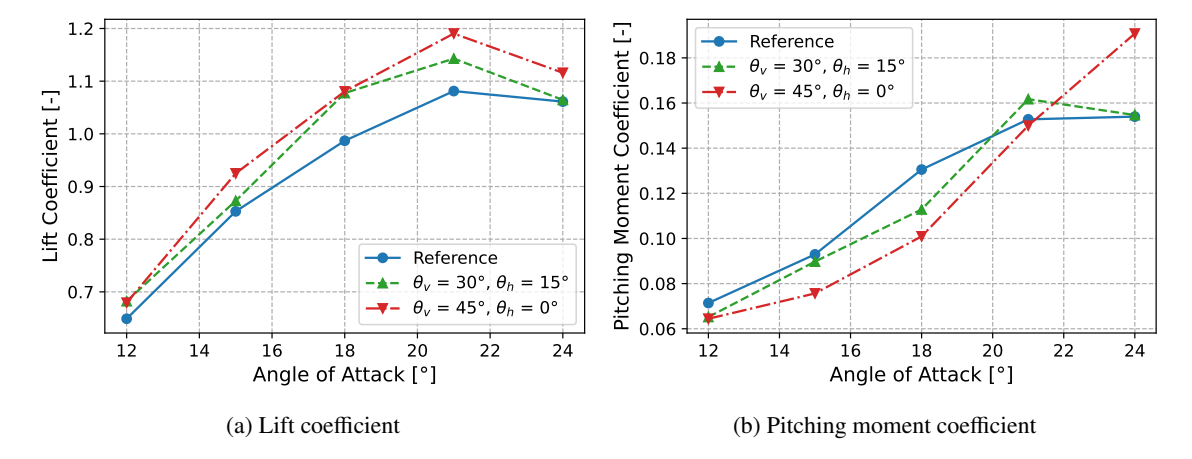


Figure 9: Comparison of the lift and pitching moment coefficient at different angles of attack for cases with and without actuation, Ma = 0.55

At Ma = 0.85, vortex breakdown is more pronounced and more abrupt than at Ma = 0.55, where the vortex breakdown starts to occur at lower angles of attack, and then only gradually moves upstream with increasing angle of attack. In contrast, at Ma = 0.85, vortex breakdown first occurs at $\alpha = 18^{\circ}$ and afterwards rapidly moves upstream with increasing angle of attack. The reason for this behaviour is the occurrence of vortex-shock interaction above the main wing, that serves to further destabilize the midboard vortex and therefore promotes vortex breakdown.

A comparison of the flow topology at Ma = 0.85, $\alpha = 21^\circ$ between simulations with and without actuation is shown in Figure 10. In the reference simulation it is visible that, at $\alpha = 21^\circ$, vortex breakdown of the midboard vortex has already progressed halfway across the wing and occurs immediately downstream of the vortex-shock interaction position. The inboard vortex is still stable, but the outboard vortex is almost non-existent. Two cases with actuation are also shown: $\theta_v = 30^\circ$, $\theta_h = 0^\circ$, $p_j = p_{s,ref}$ and $\theta_v = 45^\circ$, $\theta_h = 0^\circ$, $p_j = p_{s,ref}$. Comparing the isosurfaces, it seems that the actuation only results in a marginal delay of vortex breakdown, with the case with $\theta_v = 45^\circ$ achieving slightly better results. At Ma = 0.85, increasing the jet pressure had no positive effect on the effectiveness of the actuation.

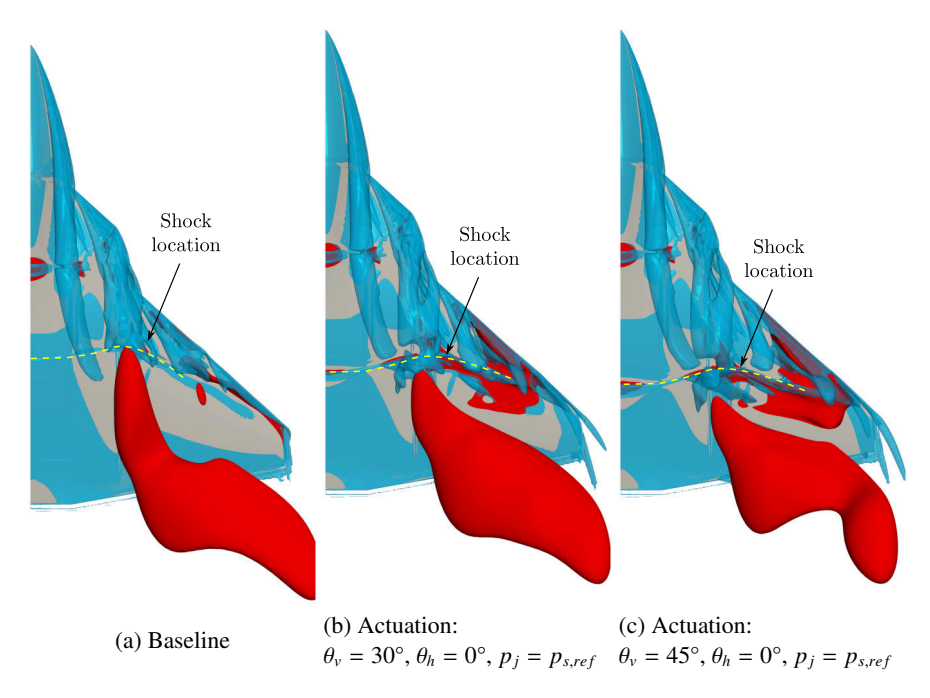


Figure 10: Visualisation of the vortex topology above the wing using an isosurface of the Q-criterion (blue) for cases with and without actuation, areas of reversed flow indicated by isosurface of $v_x = -0.1 \,\mathrm{m \, s^{-1}}$ (red), Ma = 0.85, $\alpha = 21^{\circ}$

However, by extracting and analyzing the vortex core characteristics, it becomes obvious that the actuation does result in a noticeable stabilization of the midboard vortex, as compared to the reference simulation. This is shown in Figure 11, where the development of the velocity deficit and the vorticity of the midboard vortex along the vortex trajectory is presented. As was already shown for the case at Ma = 0.55, the injection of the actuation jet results in a noticeable increase in δ downstream of the actuation position, $x \le 0.45$ m, followed by a slight re-acceleration, compare Figure 11a. The accelerated core flow stabilizes the vortex, shifting vortex breakdown downstream by $0.12c_r$ and $0.19c_r$ for the cases with $\theta_v = 30^\circ$ and $\theta_v = 45^\circ$, respectively. At the same time, the vorticity of the midboard vortex remains almost unchanged as compared to that of the reference simulation, indicating that most of the impulse of the actuation jet successfully enters the vortex core, instead of affecting the circumferential component of the midboard vortex.

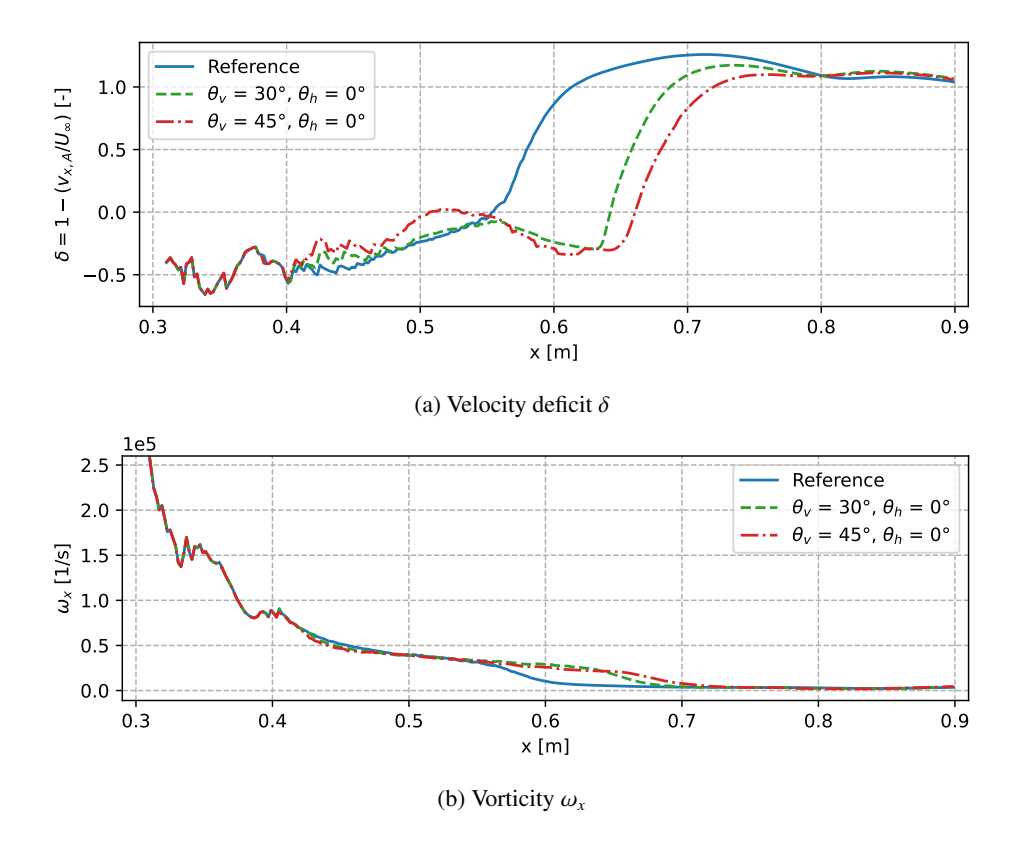


Figure 11: Comparison of the vortex core characteristics of the midboard vortex between cases with and without actuation, Ma = 0.85, $\alpha = 21^{\circ}$

The influence of the actuation on the lift and pitching moment coefficient are illustrated in Figure 12. It can be seen that both actuation settings generally achieve similar improvements to lift for $\alpha \le 21^\circ$, with a small outlier at $\alpha = 18^\circ$. However, at $\alpha = 24^\circ$, the actuation becomes completely ineffective. This is caused by the fact that the vortex breakdown position at this angle of attack is almost directly above the actuation position, so that the current actuation approach is no longer feasible. Compared to the test case at Ma = 0.55, the gains in lift are noticeably lower at between 2% to 5%. This is due to a combination of two effects: first, the size of the actuation boundary is smaller for the case at Ma = 0.85 than at Ma = 0.85, leading to a reduction in jet mass flow. Second, the ratio of the dynamic pressures of the jet and the freestream, $q_{j,eff}/q_\infty$, is smaller than at Ma = 0.55, due to the higher dynamic pressure of the freestream. Together, these effects result in about an order of magnitude difference between the blowing coefficient c_μ for the two test cases. At Ma = 0.55, the blowing coefficient is in the range of $1.34 \times 10^{-2} \le c_\mu \le 3.8 \times 10^{-2}$, whereas it is in the range of $1.2 \times 10^{-3} \le c_\mu \le 1.8 \times 10^{-3}$ at Ma = 0.85. However, increasing the blowing ratio with the current approach is not easily possible. Increasing the outlet pressure would result in the development of an underexpanded jet, that has proven to be less effective at Ma = 0.85. On the other hand, increasing the effective jet area is not feasible with the current modeling approach, as this would result in unrealistically large surface area dedicated to the actuation boundary. Instead, the most promising way forward is to actually geometrically model the actuation nozzle, and to use the outcomes of the current study as basis for the positioning and shape of the nozzle.

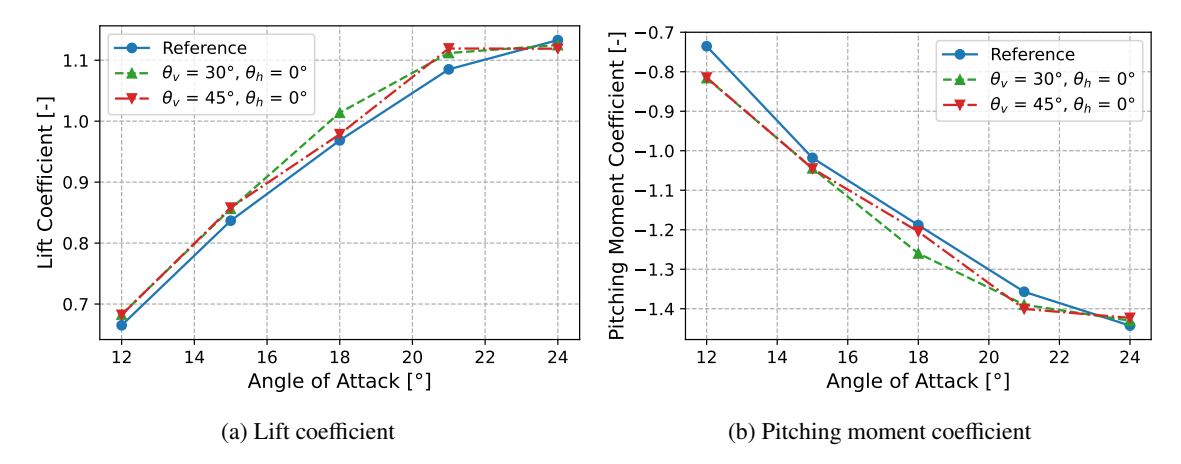


Figure 12: Comparison of the lift and pitching moment coefficient at different angles of attack for cases with and without actuation, Ma = 0.85

4. Summary and Conclusions

The use of constant blowing to delay or suppress vortex breakdown above a generic multi-swept delta wing configuration was investigated numerically. The actuation method chosen for this study was the so-called along-the-core-blowing, where a jet is used to inject additional axial momentum directly into the vortex core. Reference simulations without actuation were used to validate the CFD against existing experimental data and to identify a suitable jet position. A parametric study of the influence of jet pressure and orientation was performed at two different Mach numbers, Ma = 0.55 and Ma = 0.85, and for angles of attack between $\alpha = 12^{\circ}$ and $\alpha = 24^{\circ}$.

At Ma=0.55, the actuation proved successful in delaying or even completely suppressing vortex breakdown of the actuated vertex above the wing across the full range of investigated angles of attack. The best results were achieved by using an underexpanded jet, oriented slightly against the sense of rotation of the actuated vortex. For this case, an increase in lift of between 5% and 10% was achieved. At Ma=0.85, the actuation was less effective. Nevertheless, for $\alpha \le 21^\circ$, a delay of vortex breakdown by up to $0.19c_r$ was achieved, resulting in an increase in lift of between 2% and 5%. In contrast to the simulations at Ma=0.55, the best results were achieved for a jet with an outlet pressure matched to that of the surface pressure of the reference case. For both investigated Mach numbers, the effectiveness of the actuation drops off for higher angles of attack, once the vortex breakdown location reaches to jet location.

The reduced effectiveness of the actuation at Ma = 0.85 is attributed to the much lower blowing coefficient compared to the case at Ma = 0.55. The most promising approach to increase the blowing coefficient would be to increase the effective area of the jet. As this is not easily possible using the current approach for modeling the actuation, the next step of the investigation is to actually model the geometry of the jet nozzle. This would also serve as a useful next step in the fidelity of the simulation and hopefully allow for a more detailed comparison with subsequent experimental studies.

Acknowledgement

The authors gratefully acknowledge the scientific support and HPC resources provided by the German Aerospace Center (DLR). The HPC system CARO is partially funded by "Ministry of Science and Culture of Lower Saxony" and "Federal Ministry for Economic Affairs and Climate Action". Additionally, the authors also gratefully acknowledge the provision of the experimental iPSP data by the DLR Department of Aeroelastic Experiments.

References

- BETA CAE Systems. ANSA Pre Processor User Guide. [retrieved March 2025]. 2025. URL: https://www.beta-cae.com/ansa.htm.
- [2] T. Gerhold. "Overview of the Hybrid RANS Code TAU". In: *MEGAFLOW Numerical Flow Simulation for Aircraft Design*. Springer, Berlin, Heidelberg, 2005, pp. 81–92. DOI: 10.1007/3-540-32382-1_5.
- [3] I. Gursul and Z. Wang. "Flow Control of Tip/Edge Vortices". In: AIAA Journal 56.5 (May 2018), pp. 1731–1749. DOI: 10.2514/1.J056586.

- [4] I. Gursul, Z. Wang, and E. Vardaki. "Review of flow control mechanisms of leading-edge vortices". In: *Progress in Aerospace Sciences* 43.7 (Oct. 2007), pp. 246–270. DOI: 10.1016/j.paerosci.2007.08.001.
- [5] P. Hartl et al. "Experimental investigation of the DLR-F23 configuration at transonic speeds using fast-response pressure-sensitive paint". In: *34th congress of the international council of the aeronautical sciences, ICAS 2024*. Florence, Italy, Sept. 2024.
- [6] P. Hartl et al. "Numerical Investigation of Vortex-Breakdown Induced Tail Buffet on the DLR-F23 Configuration with Vertical Tail". In: *Jahresbericht zum 24. DGLR-Fachsymposium der STAB*. 24. DGLR-Fachsymposium der STAB. Regensburg, Nov. 2024.
- [7] S. M. Hitzel and R. Osterhuber. "Enhanced Maneuverability of a Delta-Canard Combat Aircraft by Vortex Flow Control". In: *Journal of Aircraft* 55.3 (May 2018), pp. 1090–1102. DOI: 10.2514/1.C034473.
- [8] R. B. Kurade, L. Venkatakrishnan, and G. Jagadeesh. "Control of shock-induced vortex breakdown on a delta-wing-body configuration in the transonic regime". In: *The Aeronautical Journal* 126.1299 (May 2022), pp. 768–792. DOI: 10.1017/aer.2021.99.
- [9] C. M. Liersch et al. "DLR Project Diabolo: An Approach for the Design and Technology Assessment for Future Fighter Configurations". In: *AIAA AVIATION 2023 Forum*. AIAA AVIATION 2023 Forum. San Diego, CA and Online: American Institute of Aeronautics and Astronautics, June 12, 2023. DOI: 10.2514/6.2023-3515.
- [10] O. Lucca-Negro and T. O'Doherty. "Vortex breakdown: a review". In: *Progress in Energy and Combustion Science* 27.4 (Jan. 2001), pp. 431–481. DOI: 10.1016/S0360-1285(00)00022-8.
- [11] F. R. Menter. "Two-equation eddy-viscosity turbulence models for engineering applications". In: *AIAA Journal* 32.8 (Aug. 1994), pp. 1598–1605. DOI: 10.2514/3.12149.
- [12] A. Mitchell and J. Délery. "Research into vortex breakdown control". In: *Progress in Aerospace Sciences* 37.4 (May 2001), pp. 385–418. doi: 10.1016/S0376-0421(01)00010-0.
- [13] A. Mitchell et al. "Control of vortex breakdown by along-the-core blowing". In: *Fluids 2000 Conference and Exhibit*. Fluids 2000 Conference and Exhibit. Denver, CO, U.S.A.: American Institute of Aeronautics and Astronautics, June 19, 2000. doi: 10.2514/6.2000-2608.
- [14] A. Mitchell et al. "Flow Control of Vortical Structures and Vortex Breakdown Over Slender Delta Wings". In: (2003), p. 15.
- [15] L. A. Schiavetta et al. "Shock Effects on Delta Wing Vortex Breakdown". In: *Journal of Aircraft* 46.3 (May 2009), pp. 903–914. DOI: 10.2514/1.38792.
- [16] P. P. Walatka et al. PLOT3D user's manual. Technical Memorandum 101067. NASA Ames Reasearch Center, 1990.
- [17] M. Werner, A. Schütte, and S. Weiss. "Turbulence Model Effects on Vortex Interaction Prediction on a Multi-swept Delta Wing". In: *Journal of Aircraft* 61.1 (Jan. 2024), pp. 211–221. DOI: 10.2514/1.C037421.
- [18] M. Werner et al. "Experimental and numerical analysis of the aerodynamics and vortex interactions on multi-swept delta wings". In: *CEAS Aeronautical Journal* (Aug. 26, 2023). DOI: 10.1007/s13272-023-00678-7.
- [19] J. Zastrow et al. "Numerical and Experimental Investigations on the DLR-F23 Combat Aircraft Wind Tunnel Model". In: 33rd ICAS Congress. Stockholm, 2022.